ELSEVIER

Materials Science and Engineering A356 (2003) 405–413

MATERIALS SCIENCE & ENGINEERING A

www.elsevier.com/locate/msea

Effects of tooling on the residual stress distribution in an inertia weld

J.W.L. Pang [a,1], M. Preuss [a,*], P.J. Withers [a], G.J. Baxter [b], C. Small [b]

[a] *Manchester Materials Science Centre, UMIST/University of Manchester, Grosvenor St, Manchester M1 7HS, UK*
[b] *Rolls-Royce Plc, Derby DE24 8BJ, UK*

Received 18 March 2002; received in revised form 21 October 2002

Abstract

Neutron diffraction residual strain measurements have been made on a tubular structure formed by joining two nickel-based superalloy RR1000 parts by inertia welding. Residual strains in the radial, hoop and axial directions of the tube cross-section have been measured. The corresponding residual stress field has been calculated accounting for the stress-free lattice parameter variations in the region close to the weld line. Tensile residual stresses were observed near the inner diameter of the tube with magnitudes of the order of +500, +1100 and +1300 MPa in the radial, axial and hoop directions, respectively. By comparison near the outer diameter (OD) of the weld the corresponding stresses are of the order of −200, −1000 and 150 MPa. The final stress state reflects the influence of the gripping fixture tooling and thermal gradients during inertia welding. Additional X-ray (at the surface) and hole-drilling (at the near surface) measurements show a steep residual stress gradient in the near surface region. Tensile hoop and axial machining stresses at the surface indicate the potential for improving the inertia weld tooling and the machining parameters used when removing the flash.
© 2003 Elsevier Science B.V. All rights reserved.

Keywords: Inertia welding; Residual stress; Neutron diffraction; Hole drilling; X-ray diffraction

1. Introduction

RR1000 is a recently developed powder-processed, high strength nickel-based superalloy. It is being considered for high-pressure (HP) turbine disks in the next generation of gas turbine aeroengines [1]. Nickel-base superalloys have been studied in detail for aeroengine application [2–4] in the last two decades. These alloys have shown that they have excellent creep and fatigue crack propagation properties up to 700 °C. A major difficulty to overcome for the integration of some of the next generation of nickel-based superalloys into aero-engine components is their poor weldability. Inertia welding is one of the few techniques, which can successfully join these materials with consistently low levels of non-conformance. The advantage of inertia friction welding over other welding techniques, such as electron beam welding, is the ability to weld dissimilar alloy tubular structures and conventionally difficult to weld alloys (e.g. nickel-based superalloys with a high volume fraction of γ') [5]. The process itself also solves the problem of contaminants or voids from the joint surfaces being trapped in the weld interface, as they are expelled during welding [6]. The basis of inertia welding is that one piece attached to a flywheel rotates at a large rotational speed and the stationary workpiece is forced into contact with the rotating piece under hydraulic pressure. The heat generated by friction at the rubbing surfaces provides the energy source for the weld formation without melting the material [7].

Before inertia welds can be put into commercial use, the sensitivity of the mechanical and microstructural behaviors of the joints to weld process parameters must be characterized. One important aspect that needs to be examined carefully is the development of residual stress. In a weld the parameters that determine the residual stress distribution include inertia level, axial pressure, rotational speed, the tooling and the high temperature properties of the alloy. It is known that the residual stresses in the as-welded condition can be large [8,9]. To

* Corresponding author. Tel.: +44-161-200-8959; fax: +44-161-200-3636.
E-mail address: michael.preuss@man.ac.uk (M. Preuss).
[1] Present address: Oak Ridge National Laboratory, Oak Ridge, TN 37830, USA.

0921-5093/03/$ - see front matter © 2003 Elsevier Science B.V. All rights reserved.
doi:10.1016/S0921-5093(03)00153-9

date, few strain measurements on inertia welded rings have been reported [10–12], and in most of these cases measurements have been made only along the axial direction. In addition, measurements have been made on friction stir welds [13] and linear friction welds [14], but differences between the joining geometries mean that it is not possible to carry over findings from this work. In this paper, in-depth residual stress mapping carried out at Risø, Denmark on an inertia welded tube of RR1000 is reported and analyzed.

2. Background

Inertia welding is a friction process used to join metallic components, which are symmetrical about an axis of rotation. The components to be joined are located and positioned so that their axes of symmetry coincide, such that the surfaces to be joined are parallel. One of the components to be welded is held stationary; the other is attached to a flywheel. The component-flywheel combination is accelerated to a predetermined rotational speed. The source of the rotational power is removed and the component is forced against the stationary component under a pressure, P. The inertia of the flywheel I and the rotational speed ω determine the available kinetic energy, $E = I\omega^2/2$. This kinetic energy is converted to thermal energy by friction between the components. Localized softening at the interface occurs due to the temperature increase arising from the dissipated kinetic energy. When the flywheel rotation stops, the force (pressure) between the components is maintained, permitting a bond to form at the softened interface. Cooling of the weld zone by heat conduction into the components occurs fairly rapidly after welding.

3. Experimental procedures

3.1. Sample

An inertia welded tubular structure containing a RR1000/RR1000 joint was provided by Rolls-Royce plc. The chemical composition of RR1000 [1] is listed in Table 1. This alloy belongs to the new generation of nickel-base superalloys having a significantly higher volume fraction of γ' than conventional superalloys in order to meet the demand for better high temperature properties. Since the γ' phase is $(Ni, Co)_3(Al, Ti)$, the high volume fraction of γ' is achieved by a large wt.% of Al and Ti [15]. The high volume fraction of γ' is expected to affect markedly the development of microstructure and residual stress. The RR1000 material used for this investigation came from an isothermal pancake forging, fully heat-treated and annealed. Rings with an outer diameter (OD) of 143 mm, a wall thickness of 11 mm and an axial length of 50 mm were machined from the pancake and subsequently inertia welded at MTI, South Bend, IN, USA. The dimensions of the sample after flash machining are illustrated in Fig. 1(a). For the microstructural studies a sample was machined across the weld line of a second weld joint with similar welding parameters. Preliminary studies of the γ' variation across the weld line were carried out on using a Philips XL30 FEGSEM in the secondary electron mode at 8 kV and a working distance of 10 mm. High magnification images taken at 0.3 mm from the weld line and in the unaffected parent material show the very fine (tertiary) and medium size (secondary) γ' (Fig. 2). They indicate a dramatic change of the microstructure within the near-weld zone in terms of γ' distribution and volume fraction. Within 300 μm of the weld there is only very fine tertiary (ca. 6 nm) $\gamma'$with no secondary (ca. 200 nm) or primary (ca. 1.5 μm) γ' that characterize the parent alloy. A more detailed investigation of the metallurgy in inertia welded nickel-based superalloys and its impact on residual stress measurements is described elsewhere [16].

In [8] it has been shown that the stress-free lattice spacing d^0_{hkl} is not invariant across the welded region. This variation is believed to be caused by chemical changes due to element partitioning between γ and γ' in the heat-affected zone (HAZ). The results in [8] have validated the use of an axial stress balance model to determine the stress-free lattice spacing as a function of axial distance from the weld line. This method has been applied to determine the stress-free lattice parameter in this paper.

3.2. Residual strain measurements

3.2.1. Neutron diffraction

The neutron diffraction experiment was carried out on the TAS8 spectrometer at Risø in Denmark. The 111 reflection of a pyrolithic graphite monochromator was used to provide a neutron beam of wavelength 3.000 Å. The co-ordinate system used to describe the measured

Table 1
Chemical composition (wt.%, balance nickel) of RR1000

Alloy	Cr	Co	Mo	Al	Ti	Ta	Hf	Zr	C	B
RR1000	14.35–15.15	14.0–19.0	4.25–5.25	2.85–3.15	3.45–4.15	1.35–2.15	0.0–1.0	0.05–0.07	0.012–0.033	0.01–0.025

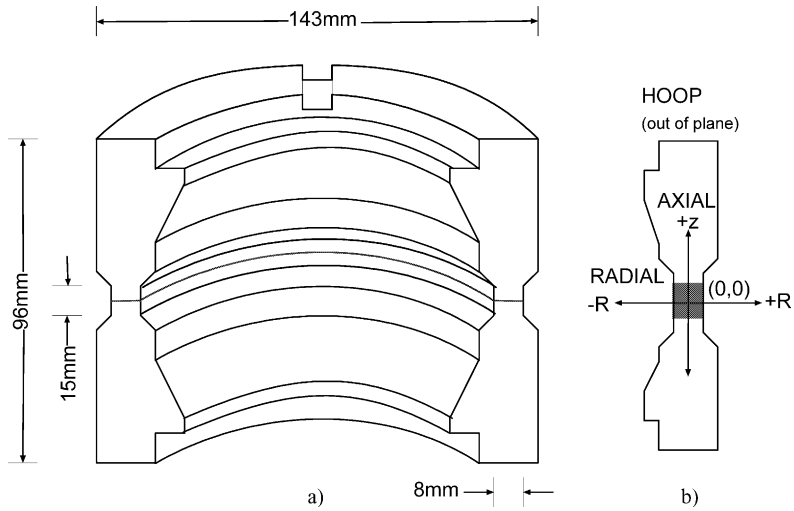

Fig. 1. (a) Cross section of the sample. The width of the weld is 8 mm. All dimensions are in millimeters; (b) the coordinate system of the measured cross section. The shaded region is the HAZ.

weld cross-section is shown in Fig. 1(b). The neutron path through the weld specimen is illustrated in Fig. 3. The gauge volume is defined by the intersection of the incident and diffracted beams. The bisector of the beams is the scattering vector Q and is parallel to the direction of the measurement. The average lattice spacing d_{hkl} of grains within the gauge volume with normal direction [hkl] parallel to Q is determined by measuring the corresponding diffracting angle. Strain is then calculated using:

$$\varepsilon_{hkl} = \frac{d_{hkl} - d^0_{hkl}}{d^0_{hkl}} \quad (1)$$

where d^0_{hkl} is the reference stress-free lattice spacing (d-zero).

When materials deform, intergranular misfit can arise causing intergranular stresses, which add to the macrostresses in which one is normally interested. In two phase materials interphase stresses can also occur due to straining incompatibilities. When the two phases are coherent, a given diffraction peak will include information about all three of these types of stress. Furthermore, the interface stresses can include coherency strains. It has been demonstrated that intergranular strain accumulation should be considered when choosing a suitable reflection for the determination of the residual stress state in an engineering component. In polycrystalline nickel-base superalloys, either the 111 or the 113 reflection make an appropriate choice of lattice reflection [17,18] because their lattice strain-applied stress curves are essentially linear even after considerable plastic strain. This makes them a good indicator of the macrostress and only weakly sensitive to the intergranular and interphase stresses. Since the counting statistics are better for the former, this one was chosen for this experiment. It has to be noted that in this work no attention has been paid to studying the different contribution of the γ and γ' phases to the 111 reflection.

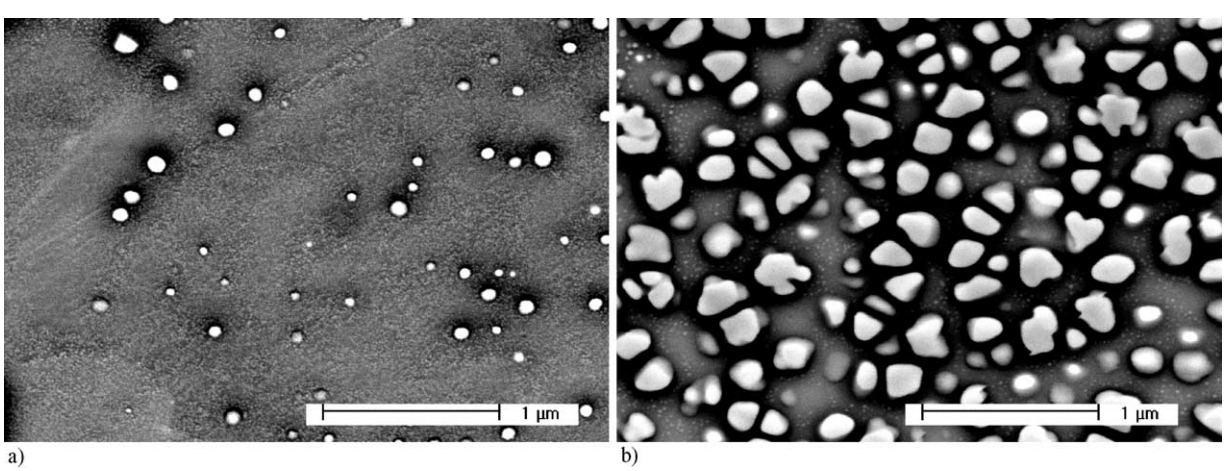

Fig. 2. SEM micrographs of (a) the region within 40 μm of the weld line ($z \approx 0$, $R \approx 0$ mm); and (b) the parent region ($z = 1.5$, $R \approx 0$ mm), of a RR1000/RR1000 inertia weld.

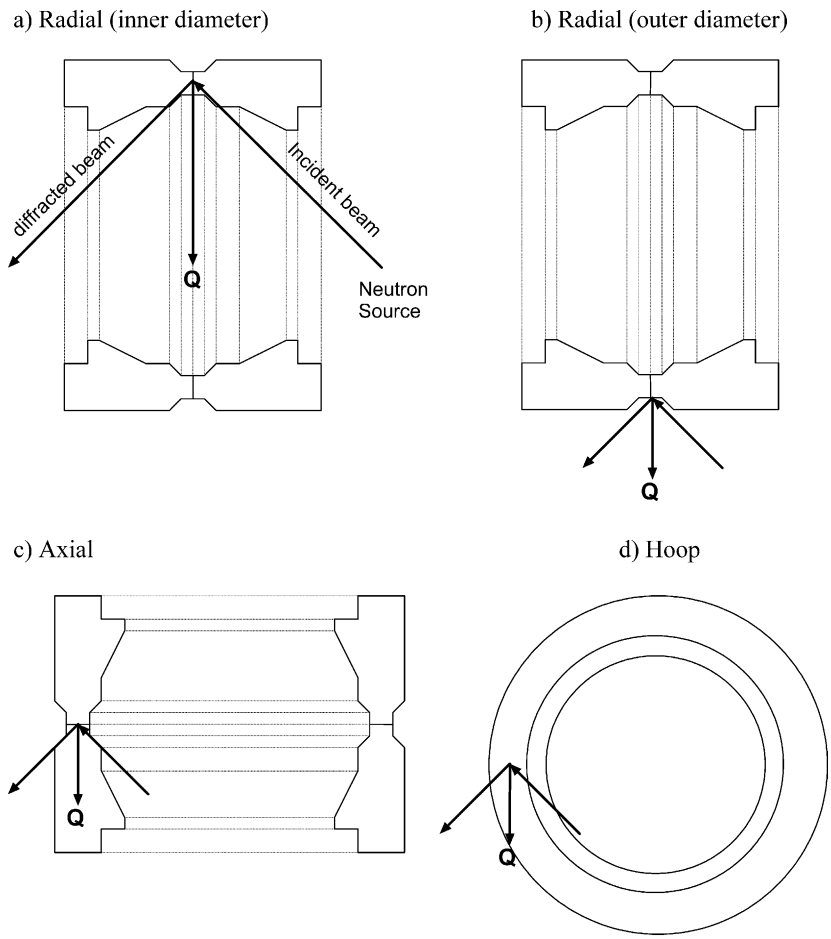

Fig. 3. Orientations of the specimen with respect to the neutron beams for radial, axial and hoop strain components. The gauge volumes for the radial and axial measurements are 10(H) × 1(W) × 1(D) mm^3. The gauge volumes for the hoop measurements are 5(H) × 2(W) × 2(D) mm^3 and 2(H) × 2(W) × 2(D) mm^3.

As the intragranular γ' particles are coherent with the matrix (γ), both phases contribute to the 111 reflection and a change of the γ' volume fraction (as observed here) and a change of the stress state between the two phases can potentially have an impact on the 111 reflection and might result in a change of the overall 111 lattice parameter. Since this experiment was carried out under an engineering approach and beam time on TAS8 was limited it was not possible to resolve the contribution of both phases as has been done in the past [18]. Since an axial macrostress balance was imposed as part of the d-zero determination, as described in Section 4.1, any change in the contribution of the γ' reflection to the overall 111 reflection will not affect the macrostrain measurements significantly. However, at the weld line, the macro stresses are mainly determined by the γ phase, whereas in the parent materials it is the γ and γ' phase. This might have an impact on the overall measured stress distribution, since the emphasis is shifted to one phase. But since both phases are exposed to the same macro residual stresses, this should have only a minor affect on the strain calculation when an axial stress balance is used. Measurements were concentrated in the HAZ. The orientations of the sample with respect to the neutron beams for radial, axial and hoop strain components are shown in Fig. 3. Since for thermal neutrons a neutron path length of 10 mm in nickel will reduce the diffracted beam intensity by $\sim 80\%$ (the linear absorption coefficient of Ni is 0.25 cm^{-1} [19]), the sample was oriented to achieve the shortest possible path length at all times.

In the case of the radial and axial strain measurements, the size of the neutron beam used was 1 mm wide in order to give good spatial resolution in the axial direction but 10 mm in height to give good counting statistics. Therefore, the measurements taken were averages over an arc distance of $\sim 8°$. Since all measurements were made at least 1 mm inside the outer and inner surfaces of the weld, the variation of residual strains over such a small arc distance is not expected to be large. Line scans along z were made through the thickness of the weld at $R = -3$ mm (close to inner

diameter), −1 mm, 0 mm (center), 1 mm, 3 mm (close to OD). The uncertainties of the strain measurements were about 100 με (1 $\mu\varepsilon = 10^{-6}$) on average. Because of the geometry of the sample, hoop strains were measured by placing the sample flat on the translator table with its rotating axis lying perpendicular to the neutron beams. The path length was about 23 mm, which is at least twice that for the radial and axial components. For the hoop strains, line scans were made at $R = -3$, −1.5, 0, 1.5 and 3 mm using a gauge volume of 5(h) × 2(w) × 2(d) mm^3. Plotted against the axial position, these data points could be fitted to a second order polynomial distribution. Strains for positive z have also been determined with a $2 \times 2 \times 2$ mm^3 gauge volume for higher spatial resolution at $R = -2$, 0 and 2 mm. Due to the long path lengths and small gauge volumes, counting times up to 8 h were required for a single measurement to achieve a hoop strain uncertainty of 300 με. Therefore, only three linescans were carried out and strain data had to be inter/extrapolated in order to calculate the residual stresses at $R = -3$, −1.5, 0, 1.5 and 3 mm. The extrapolation was carried out by using the second order polynomial obtained from the first line scan in the hoop direction using the large gauge volume. For the stress-free lattice spacings d^0_{hkl}, thin slices of post weld heat treated material were stacked together and the average lattice spacings were measured in the radial, hoop and axial directions at different locations using a gauge volume of 2(h) × 2(w) × 2(d) mm^3. Since an axial stress balance model was applied to infer $d^0_{hkl}(z)$ when calculating the residual stresses, the global stress-free lattice spacing d^0_{hkl} measured in this way was not used, however, it compared well with the calculated stress-free lattice spacing corresponding to the parent material. It is worth noting that applying an axial stress balance to infer $d^0_{hkl}(z)$ has certain advantages especially in respect of minimizing the possible impact of the γ' phase on the peak position as mentioned above.

3.2.2. Hole-drilling

Neutron diffraction strain measurements made very near to the surface are vulnerable to serious errors, when the gauge volume is not fully immersed in the bulk material [20]. The recorded diffraction peak is a statistical distribution of the contributions from all the diffracting crystals in the gauge volume. When the gauge volume is only half immersed in the material, the statistical distribution of the diffraction peak is changed and results in a so-called geometrical pseudostrain [21]. Therefore, hole-drilling is a more appropriate technique for near surface residual stress measurements. Residual stresses have been determined from strain measurements using the target strain gauge/center hole drilling technique (diameter of the drill 0.9 mm) to a maximum depth of 0.64 mm from the surface. Three sets of gauges have been installed in 120° angular locations to each other at the outer surface of the weld line. The integral method, which is based on a linear elastic model, was used to calculate the hoop and axial residual stresses from the strain changes during hole-drilling.

3.2.3. X-rays

Laboratory X-rays sources have very low surface penetration (typically ≈ 15 μm) into nickel making them ideal for surface measurements of the residual stresses. The measurements were carried out at Rolls-Royce plc. A TEC 1620-2b X-ray stress analysis system was used with an iron target X-ray source at 35 kV and 1 mA. Using the FeK_α radiation on the 311 reflection, measurements were carried out in a 2θ of about 126.4°. In order to measure the hoop and axial residual stresses at the outer surface of the weld line, the $\sin^2 \Psi$ technique, as described by Cullity [22], was employed. The location of the diffraction peaks 2θ were converted to lattice spacing d using Bragg's law. Residual stresses σ_S were then calculated using the following equation:

$$\sigma_S = \frac{E}{(1+\nu)\sin^2 \Psi}\left(\frac{d_\Psi - d_n}{d_n}\right) \quad (2)$$

where d_ψ is inclined at angle ψ to the surface normal, d_n is parallel to the surface normal and E and ν are the diffraction elastic constants (DEC) of the lattice plane under consideration. Eq. (2) assumes that the out-of-plane stress is zero, which, by definition, is the case at the surface [23]. As mentioned above, the penetration depth of X-rays in nickel-base superalloys is small, limiting the measurements to a few microns beneath the surface. Therefore, the assumption for Eq. (2) is appropriate, even when large stresses are observed in the near surface region. If no shear stress component is apparent, a linear regression of d_ψ versus $\sin^2 \psi$ provides the best estimate of the gradient $\sigma_s d_n(1+\nu)/E$ and a knowledge of the appropriate DECs infers σ_S. The measurements carried out on the inertia-welded sample showed no shear stress component (best fit for d_ψ vs. $\sin^2 \psi$ is a linear regression) and, therefore, only the positive ψ range with ψ angles of 0, 15, 24, 35 and 45° were employed. It has to be noted that the limited ψ range may give a large uncertainty for the stress calculation when steep stress gradients at the surface are apparent. For the 311 reflection the DECs of $E =$ 224 GPa and $\nu = 0.24$ were used [14]. Typical stress measurement uncertainties were around ±100 MPa.

4. Results

4.1. Neutron diffraction

For strain calculations, d^0 was determined as a function of axial position from axial stress balance as

described in [8], resulting in a lattice spacing of 2.0768 Å at the weld line and 2.0765 Å in the parent material. The d-zero variation is only significant within about 4 mm from the weld line. The change of d-zero across the weld line was significantly smaller than presented in [8], which reports neutron diffraction measurements on a very similar inertia welded sample but measured with a higher spatial resolution. A large gauge volume during hoop measurements, as necessary during this experiment (here $2 \times 2 \times 2$ mm^3 whereas in [8] it was $2 \times 1 \times 1.5$ mm^3), smears out the localized d-zero variation observed in inertia welded nickel superalloys [8]. Therefore, using larger gauge volumes during the measurement of the radial, axial and hoop strains, makes the residual strains less susceptible to d-zero shifts but does flatten the measured stress variation somewhat.

The radial, axial and hoop residual strain profiles are shown in Fig. 4. At all depths the radial strain is largest near the weld line ($z = 0$ mm), and the responses are essentially symmetric about $z = 0$, as one might expect. A compressive peak value of 1500 ± 200 με is observed for the radial measurements near the innermost diameter at the weld line. Near the outermost diameter the radial strains are tensile, but smaller in magnitude.

Over the range of measurements, the axial strains are essentially independent of z, but vary markedly with radial position. In view of this, the axial strains have been averaged for each R value and are plotted in Fig. 5. The axial strain varies approximately linearly with depth from a tensile strain of 2300 ± 100 με to a compressive strain of -3000 ± 200 με from the inner to the ODs. At the mid-wall thickness ($R = 0$ mm), the axial strain is approximately zero. Such a strain variation is indicative of a bending moment. As for the other two strain components, the through thickness hoop strains are symmetric about the weld line. Measurements with the smaller gauge volume show that the hoop strains are tensile and decrease with distance from the weld line and are largest near the inner diameter.

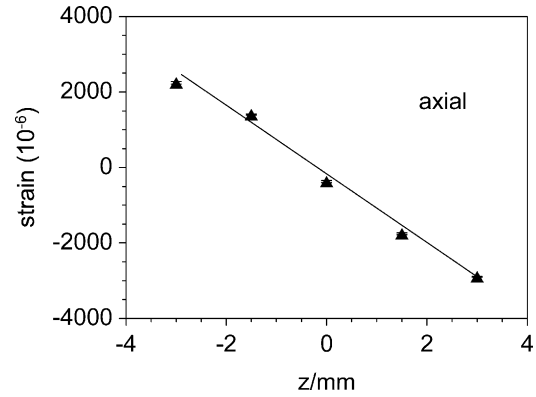

Fig. 5. Axial component of the residual strain field averaged over z and plotted as a function of R only.

The axial, hoop and radial residual stresses at the weld line were calculated using variants based on the following equation:

$$\sigma_{axial} = \frac{E}{(1+\nu)(1-2\nu)} \times [(1-\nu)\varepsilon_{axial} + \nu(\varepsilon_{radial} + \varepsilon_{hoop})], \text{ etc.} \quad (3)$$

where E and ν are the DECs and the Poisson's ratio for reflection 111 and their values are 267 GPa and 0.36 [24], respectively. Given the symmetry about the weld line, the radial strains were averaged (in pairs) about $z = 0$ to improve the statistics for the calculated stresses. Averaged axial strains (see Fig. 5) and hoop strains determined with the smaller gauge volume were used for the stress calculations. The residual stresses for the radial, axial and hoop components at the weld line are shown in Fig. 6 as a function of R. Due to the relatively large errors in the hoop strains, uncertainties of the calculated residual stresses are about ± 70 MPa in the

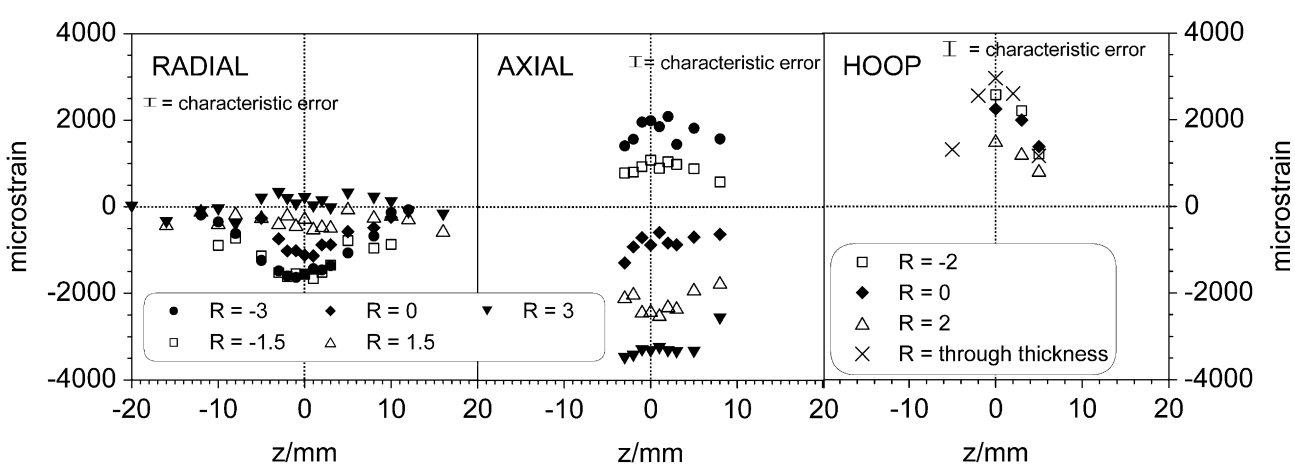

Fig. 4. Residual strain profiles of the tube cross section as a function of axial distance from the joint. In the radial direction the inner and outer radii are at -4 and $+4$ mm, respectively, and z, are from the weld line in the axial direction.

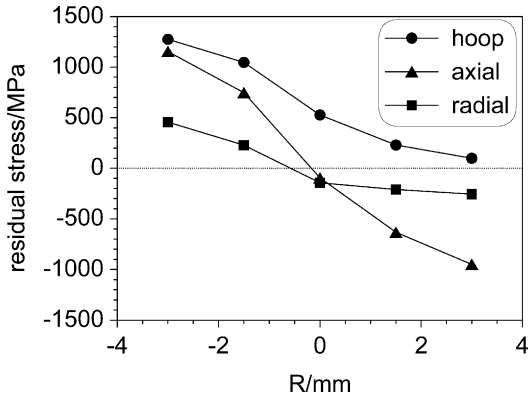

Fig. 6. The calculated radial, axial and hoop residual stresses at the weld line as a function of the radial position R.

radial and axial directions and ± 100 MPa in the hoop direction. The hoop stress field exhibits the largest tensile stresses with about 1300 MPa at the weld line close to the inner diameter. In this region, a hydrostatic stress component (≈ 1000 MPa) is apparent with the hoop, axial and radial directions all stressed in tension. Since the measured residual stresses are very large, it is useful to compare the stress data with the yield stress of the material (1050 MPa). Using the Tresca yield criterion the difference between the maximum and minimum stress components is 800 MPa, just below the yield stress.

4.2. Hole-drilling and X-ray measurements

The near surface hole drilling and surface X-ray hoop and axial measurements are plotted alongside the neutron diffraction measurements in Fig. 7 measured at the weld line of the sample ($z = 0$). The X-ray measurements reveal significant tensile stresses in the hoop and axial direction, 500 and 800 MPa, respectively, at the surface. The d versus $\sin^2 \psi$ plot displayed linearity, indicating zero out-of-plane stress for the measured volume (penetration depth < 10 μm). These results are in line with the hole-drilling measurement points closest to the surface of the sample. However, since only a limited ψ range was measured (45°), the X-ray results should be treated with some care. The hole-drilling results indicate that just below the surface the strains vary steeply. Just 100 μm beneath the surface ($z = 3.9$ mm), the axial stresses exhibit a large drop into compression (-1400 MPa). Beyond this depth, the axial residual compressive stresses measured by hole drilling and then neutron diffraction fall sharply towards zero near the mid-radius before rising to a tensile maximum near the inner diameter. In the same region the hoop stresses increase from zero to about 1500 MPa towards the inner diameter. Especially for the axial measurements, good continuity between hole-drilling and neutron diffraction results are observed. Because of the access problems associated with the small radius of the welded tube it is very difficult to make hole drilling or X-ray measurements near the inner diameter, where the bulk measurement indicate the largest tensile stresses.

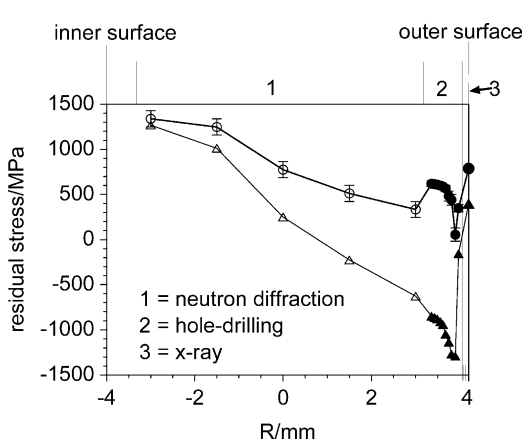

Fig. 7. Axial and hoop residual stresses at the weld line comprising neutron diffraction (region 1), hole-drilling (region 2) and X-ray (region 3) results. The residual stresses are plotted as a function of the radial position (R).

5. Discussions and conclusions

Residual stress mapping has been made non-destructively across the cross-section of an RR1000/RR1000 inertia weld. Large tensile residual stresses were found near the inner diameter for all three components. In this location the equivalent stress is very close to the yield stress. During welding, heat generated by the friction process causes the weld material to soften and expand. Upon joint formation, large tensile hoop stresses develop because the contraction of the weld zone is retarded. This is characteristic of many welding methods. The strong variation in axial stress across the section is almost certainly a consequence of the constraint imposed by the tooling in order to hold the tube sections in place during welding. Clamping of the unwelded ends appears to have introduced large bending forces on both pieces. When the clamps are removed after welding, the bending forces would relax but for the constraining influence of the weld just formed, as illustrated in Fig. 8. This in turn leads to the development of residual axial stresses. The low z-dependency of the axial stresses compared with the radial and hoop stresses also suggests that their origin lies not in the thermomechanical history of the weld locality, as is the case for the hoop and radial stresses, but in the longer range jigging influence of the tooling.

The combination of neutron diffraction, hole-drilling and X-ray measurements shows the ability to record the

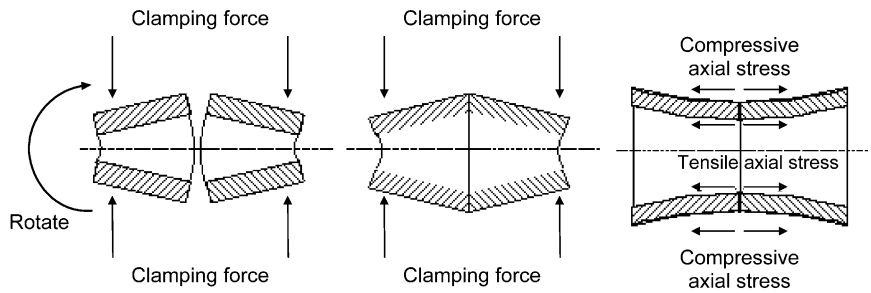

Fig. 8. Schematic diagram to illustrate the development of axial residual stresses due to tooling: (a) the two pieces are clamped and are bent; (b) the clamping forces are still applied during welding; and (c) the clamps are removed—the two ends of the weld are fully relaxed and axial stresses are developed in the welded area.

complete residual stress field from the surface into the bulk material for the hoop and axial directions. Large tensile machining stresses were measured at the surface of the weld line. The problem of tensile stresses at the surface may be even more important on the inner diameter for which the welding process generates significant tensile macro residual stresses. It might be possible to minimize the tensile stresses at the surface by optimizing the tooling and the process parameters for removing the weld flash. In further investigations, X-ray measurements will help to study the surface stresses around the weld line. Since a good continuity is observed between the hole-drilling and neutron diffraction results, the hole-drilling results corroborate the neutron diffraction measurements close to the outer surface. In further investigations the hole-drilling technique will be adopted to measure the axial and hoop residual stresses at the inner diameter [25]. The effects of tooling on the axial stresses are larger than those of the welding parameters. The measurements suggest that it is necessary to consider clamping forces as a boundary condition in any finite element modeling of the welding process. Careful studies on the sensitivity of residual stress development to welding parameters are essential for successful application of the inertia welding technique for the production of aeroengine components.

As this work shows, neutron diffraction strain mapping can be used in order to chart the residual stresses introduced during the welding process. Hole-drilling results can give information about the near surface stress field and an indication of the bulk residual stress in the axial and hoop direction. X-ray measurements can highlight problematic tensile stresses at the surface and will be used in the future to help optimize the tooling and the process parameters for removing the weld flash, however, values measured at the surface are quite unrepresentative of the bulk due to steep near surface strain gradients.

Acknowledgements

The authors would like to thank Dr T. Lorentzen and C. Klitholm (Risø) for experimental assistance during neutron diffraction measurements. The European Large Installations Programme supported the funding for beam time. This project was financially supported by EPSRC and Rolls Royce Plc.

References

[1] S.J. Hessell, W. Voice, A.W. James, S.A. Blackham, C.J. Small, M.R. Winstone, Nickel alloy for turbine engine components, United States patent number 5897718 (27 April 1999).
[2] J.P. Perte, J. Phys. IV Colloque C7 3 (1993) 1019–1027.
[3] J.Y. Guedou, J.C. Lautridou, Y. Honnorat, Rev. Sci. Snecma 5 (1994) 53–61.
[4] D. Locq, M. Marty, P. Caron, in: T.M. Pollock, R.D. Kissinger, R.R. Bowman, K.A. Green, M. McLean, S.L. Olson, J.J. Schirra (Eds.), Superalloy 2000, The Minerals, Metals and Materials Society, Warrendale, 2000, pp. 395–403.
[5] E.D. Nicholas, W.M. Thomas, Int. J. Mater. Prod. Technol. 13 (1998) 45–55.
[6] K.K. Wang, Welding Res. Council Bull. 204 (1975) 1–22.
[7] Y.P. Lei, Y.W. Shi, J. Mater. Process. Technol. 44 (1994) 265–272.
[8] M. Preuss, J.W.L. Pang, P.J. Withers, G. Baxter, Metall. Mater. Trans. A 33 (2002) 3227–3234.
[9] M. Preuss, A. Steuwer, P.J. Withers, G.J. Baxter, S. Bray, in: ASM International Sixth International Trends in Welding Research Conference, Pine Mountain, USA, April 2002, in press.
[10] M.E. Abdel Moniem, S.M. Serag, A.A. Nasses, A.A. Moustafa, Wear 70 (1981) 227–241.
[11] H.G. Priesmeyer, J. Schroeder, in: H. Fujiwara, T. Abe, K. Tanaka (Eds.), Residual Stresses—III: Science and Technology, Elsevier, London, 1992, pp. 253–258.
[12] H.U. Baron, V. Schlett, in: K.H. Rendigs, P.J. Winkler (Eds.), Third International Conference on Welding in Aerospace Industry, German Welding Society, Essen, 1993, pp. 114–117.
[13] X.L. Wang, S.A. David, S. Spooner, C.R. Hubbard, Z. Feng, in: G.A. Webster (Ed.), Sixth Conference on Residual Stresses (ICRS-6), IOM Communication, London, 2000, pp. 1408–1414.

[14] N.W. Bonner, A.N. Ezeilo, in: G.A. Webster (Ed.), Sixth Conference on Residual Stresses (ICRS-6), IOM Communications, Oxford, 2000, pp. 1385–1392.
[15] C.T. Sims, W.C. Hagel (Eds.), The Superalloys, Wiley, New York, 1972, pp. 43–46.
[16] M. Preuss, J.W.L. Pang, P.J. Withers, G. Baxter, Metall. Mater. Trans. A 33 (2002) 3215–3225.
[17] T.M. Holden, R.A. Holt, A.P. Clarke, Mater. Sci. Eng. A246 (1998) 180–198.
[18] H.J. Stone, T.M. Holden, R.C. Reed, Scr. Mater. 40 (3) (1999) 353–358.
[19] G.E. Bacon, Neutron Diffraction, third ed, Clarendon Press, Oxford, 1975, p. 72.
[20] P.J. Webster, G. Mills, X.D. Wang, W.P. Kang, T.M. Holden, J. Neutron Res. 3 (1996) 223–240.
[21] D. Wang, I.B. Harris, P.J. Withers, L. Edwards, in: S. Denis, J.-L. Lebrun, B. Bourniquel, M. Marral, J.-F. Flavenot (Eds.), ECRS-4, Société Française de Métallurgieet de Matériaux, Cluny en Bourgogne, 1996, pp. 69–78.
[22] B.D. Cullity, Elements of X-ray Diffraction, second ed, Addison-Wesley, London, 1978, pp. 447–478.
[23] I.C. Noyan, J.B. Cohen, Residual Stress, Measurements by Diffraction and Interpretation, Springer, New York, 1987, pp. 140–144.
[24] A.N. Ezeilo, G.A. Webster, P.J. Webster, X. Wang, Phys. B: Condens. Mater. 180-181 (1992) 1044–1046.
[25] G.J. Baxter, M. Preuss, P.J. Withers, in: International Conference on The Microstructure and Performance of Joints in High-Temperature Alloys, London, UK, Science Technology Welding Joining (November 2002), in press.